Journal of Archaeological Science: Reports 32 (2020) 102396

Contents lists available at ScienceDirect

Journal of Archaeological Science: Reports

journal homepage: www.elsevier.com/locate/jasrep

Comparing traditional and virtual approaches in the micro-excavation and analysis of cremated remains

Owen Alexander Higgins[a,1,*], Antonino Vazzana[a,1], Lucia Martina Scalise[a], Federica Maria Riso[b], Laura Buti[a], Sara Conti[a], Eugenio Bortolini[a], Gregorio Oxilia[a], Stefano Benazzi[a]

[a] Department of Cultural Heritage, University of Bologna, Italy
[b] Department of History and Cultures, University of Bologna, Italy

ARTICLE INFO

Keywords:
Cremated remains
Computed tomography
Digital micro-excavation
Volume rendering
Roman Empire
Italy
Mutina

ABSTRACT

The excavation and micro-excavation of archaeological contexts are, and always have been, destructive operations by definition. This study, although preliminary, has allowed the experimentation and application of computed tomography and engineering softwares (used for the creation and manipulation of three-dimensional surfaces) in micro-stratigraphic archaeological excavations, with the objective to overcome the very destructiveness that is intrinsic to the traditional method. For this purpose, a Roman cremation urn from the monumental necropolis in Via Emilia est – Tangenziale Pasternak (Modena) was chosen as a test subject. The application of this approach consented the analysis of both context and remains as close as possible to their original condition, exhibiting minor fragmentation in comparison with the traditional method which in turn allowed a clearer determination of the individual's biological profile. Moreover, also in virtue of the observation of elements which were not detected by the traditional method, virtual micro-excavation is to be considered a promising approach for the investigation of particular archaeological contexts, enabling greater preservation and enhancing both documentation and analysis.

1. Introduction

Archaeology is a work of destruction. This is an important lesson that each aspiring and future archaeologist has had to learn from the beginning, since an archaeological excavation has always been an unrepeatable process and all unrecorded data would be lost forever. Although on an extensive scale this paradigm may still be mostly valid, the destruction of smaller contexts may be avoided by resorting to computed tomography (CT) and virtual technology.

Since a cremation urn is «a tiny archaeological site of its own, with finds, features, stratification and structure» (Minozzi et al., 2010), one was specifically chosen for this study. The urn's limited dimensions and enclosed space allowed the context to be easily extracted, transported and scanned, whereas the notorious fragmentation and brittleness of its burned remains offered a good comparison to test the potentialities of the here-proposed new approach.

In fact, due to the destructiveness of the cremation process and to the consequential fragmentation of the remains, the analysis of cremated bones can be challenging and often delivers scarce results (Hamilton and Green, 2017). Furthermore, cremated bones also undergo supplemental fragmentation after deposition – due to soil pressure, changes in temperature and moisture (McKinley, 1994; Waterhouse, 2013) – and during both the excavation and the cleaning procedures, adding further difficulties to an already challenging situation.

This is not the first time CT has been used on cremated remains (Anderson and Fell, 1995; Cavalli et al., 2015; Harvig et al., 2012; Minozzi et al., 2010; Pankowská et al., 2014; Vincenzutto et al., 2016), but it is seldom applied and has been supplemented with three-dimensional (3D) virtual technology only in isolated attempts (Cavalli et al., 2015; Harvig et al., 2012; Minozzi et al., 2010).

This study combines the two tools and brings their use a step further by conducting a digital micro-excavation of an archaeological context within a funerary urn and an anthropological analysis on the virtual remains. In addition, the urn was also micro-excavated and analysed by a second operator using traditional methods, in order to explore strengths and weaknesses of the two different approaches.

2. Material

The urn which was here chosen as a test subject was extracted in

* Corresponding author.
E-mail address: owen.a.higgins@gmail.com (O.A. Higgins).
[1] These authors contributed equally.

https://doi.org/10.1016/j.jasrep.2020.102396
Received 31 January 2020; Received in revised form 13 April 2020; Accepted 2 May 2020
Available online 11 May 2020
2352-409X/

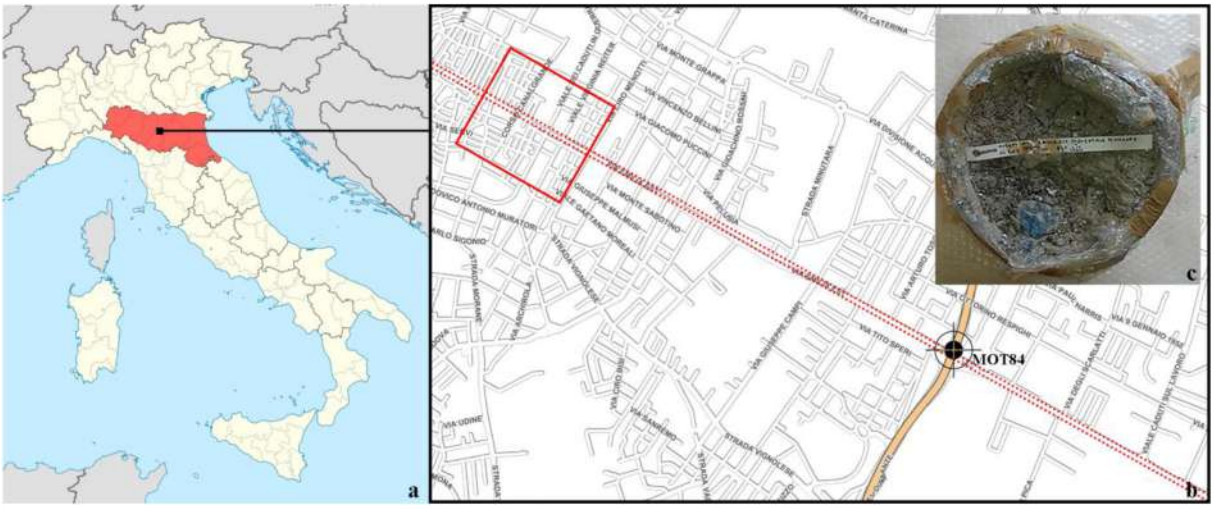

Fig. 1. a) Map indicating the location of Modena (in red, the region Emilia-Romagna); b) Detail of modern Modena (the crosshair indicates the location of the site; the red square indicates the limits of ancient *Mutina*; the double-dotted red line indicates the *via Aemila*); c) Picture of tomb 10.

2007 by the Superintendence of Archaeology, Fine Arts and Landscape of Emilia-Romagna (a section of the Italian Ministry of Cultural Heritage and Activities and Tourism) during a commercial archaeology campaign at the intersection between *via Emilia* and *Tangenziale Pasternak*, in Modena, Italy. The roadworks unearthed a segment of the Roman *via Aemilia* and the monumental necropolis that runs along it. In the specific, the archaeological investigation regarded a sector (MOT84) set orthogonally to the *via Emilia* at *circa* 2 km from the centre of the ancient *Mutina* (Fig. 1a, b). The excavation reached a depth of *circa* 5.5 m, revealing the alternation of natural and anthropic layers which occurred in the time between the Roman period and modern days. A total of 15 cremation tombs – dated between the ~~I~~ 1st and the first half of the ~~II~~ 2nd century CE – were investigated during the archaeological campaign. They were arranged following a linear progression along the road and were grouped in six distinct funerary complexes (areas 1, 2, 3 and 5 on the northern side of the road and areas 4 and 6 on the southern side).

The test subject chosen for this study is tomb 10, from funerary area 2. The urn is a brick-red, coarse-grained ceramic *olla* of 22 cm in height, with an ovoid body, an everted lip and a flat base (Fig. 1c). It was deposited in a circular pit of 50 cm in diameter, with a concave profile and oblique walls, that cut an alluvial layer with a loamy-clayey matrix. The urn was partly covered by a clayey (slightly loamy) layer with many clumps of burnt soil and charcoal and partly by a loamy-clayey layer which was instead abundant with clumps of burnt soil and charcoal. Next to the urn were found: a beige ceramic oil lamp with a triangular nozzle, a molten glass unguentarium and a bronze Aucissa-type fibula.

3. Method

This study was conducted as a double-blinded experiment, by compartmentalising it into two parallel and independent segments: on one side the traditional method, and on the other the virtual approach. This course of procedure favoured the elimination of possible biases while carrying out the individual approaches, later allowing an unimpaired comparison of both methods on their completion.

3.1. Traditional approach

3.1.1. Physical micro-excavation

The physical micro-excavation was conducted at the Museo Civico Archeologico di Modena. Due to the absence of a general and codified methodology for micro-excavation, different studies can be taken as a reference for this operation (Casu and Cagnini, 2016; Cavazzuti and Salvadei, 2014). After a complete photographic documentation, the micro-excavation was carried out in horizontal layers from the top downwards by removing 2 cm of material at a time (except for layer n. 3 which was 4 cm deep). This gave nine fairly regularly-distanced cuts that were each measured, described and photographically documented (see Appendix A). The extracted material was sorted per layer and sieved with water by piling sieves in decreasing link-size order (10, 0.5, 0.2 mm), with the smallest one being used for subsequent carpological and anthracological studies. The finds were left to dry directly in the sieves in a dry area away from direct light and heat.

3.1.2. Traditional anthropological analysis

The bone elements were then transferred to the "Osteoarchaeology and Palaeoanthropology laboratory (BONES Lab)" of the department of Cultural Heritage of the University of Bologna in Ravenna (Italy) where they were cleaned and left to dry away from direct light and heat.

By maintaining the division according to layer, each element was identified and sorted according to type of material: pottery, glass, human or animal bone fragments. The bone fragments were determined and the elements which could not be determined were divided according to the maximum degree of identification possible: epiphyseal fragments, diaphyseal fragments, trabecular bones or indeterminates (France, 2010; White and Folkens, 2005).

The presence and the incidence of the various anatomical districts in each layer was calculated in order to determine whether there might have been an intentional or accidental order of deposition. Furthermore, a phase of combustion was attributed to each fragment to generally define the evolution of this process, not to identify specific temperatures of combustion. The attribution was based on the observed colour, which was determined by comparing the NCS INDEX®© 1950 colour chart to the table in Walker et al. (2008) under a white (40 W) light and a homogeneous light distribution. The phases that were taken into account are: phase 1 (unburnt to ca. 300 °C), phase 2 (ca. 350 to 600 °C), phase 3 (ca. 600 to over 1000 °C) and the pertaining intermediate phases 1–2 (ca. 300 to 800 °C) and 2–3 (ca. 600 to 800 °C), which were made necessary due to the absence of a clear distinction between one stage and the other. Phase 4 (identifiable as the stage of fusion) was not taken into account since the colour of the bone corresponds to the one assumed during the previous phase (inversion) (Thompson et al., 2017). Whether there was presence of different colours on the same fragment, the latter was attributed either based on the predominant colour or – if there was not a predominant colour – to the corresponding intermediate phase.

Subsequently, the fragments from all layers were united and laid out according to their anatomical position. The percentage of fragments and the combustion phases identified for each anatomical element of the human remains were then calculated.

Finally, in order to determine the biological profile of the individual, the methodologies were selected based on the preserved diagnostic districts. For sex estimation, the works of Acsadi and Nemeskeri (1974) and Cavazzuti et al. (2019) were taken into consideration. Whereas the weight of the cremated remains was not considered due to the controversiality of such method, whose results are susceptible to countless variables (Gonçalves et al., 2013). Observations regarding estimation of age at death were carried out by following the morphological criteria described by Buikstra and Ubelaker (1994) and Brooks and Suchey (1990). Whereas the presence of pathological conditions was evaluated by referring to the work of Ortner (2003).

3.2. Virtual approach

3.2.1. Data acquisition, segmentation/micro-excavation and surface creation

Before the traditional micro-excavation took place, the urn and its contents were scanned by TEC-EUROLAB in Campogalliano (MO) with an NSI X7500 CT System scanner, using the following scanning parameters: 450 kV and 1570 μA. The CT scan files were saved in DICOM format at a reconstructed matrix size of 150 μm voxels.

The CT image data was manually segmented using Avizo Lite 2019.1 software (Thermo Fisher Scientific, Waltham, Massachusetts, USA), in order to reconstruct the 3D models of the finds. This process consists in the identification, selection and labelling of each relevant structure by hand, referring only to the spectrogram and to the differences in density - rendered in grey level Hounsfield Units - that are distinguishable by naked eye (Chityala et al., 2013; Godinho and O'Higgins, 2017; Suuronen et al., 2013; Villinger et al., 2012).

Manual segmentation – rather than automatic segmentation – was made necessary by the poor contrast that characterised the slices (tomographic images), which did not allow the identification of a threshold able to discern one class of material from the other, including the sediment. However, it was possible to identify separate thresholds for single elements, which did allow a more accurate segmentation.

Due to the extended time that is required by manual segmentation of such large and complex data, it was decided to focus on the recognisable and most diagnostic elements, postponing the detection of a more refined and swifter working methodology to further studies.

During the segmentation process, each element was labelled as a separate material and then exported in little-endian format (.stl) by ensuring the conservation of the relative location and orientation of every element. This step was necessary in order to extract the 3D digital models that were then uploaded in Geomagic Design X (3D Systems, Rock Hill, South Carolina, USA) to carry out the optimisation of the surfaces (Benazzi et al., 2016, 2015; Godinho and O'Higgins, 2017; Traversari et al., 2019; Vazzana et al., 2018).

3.2.2. Virtual anthropological analysis

The complexity that characterised the contents of the urn and the partial segmentation of the bones, did not allow the count of the total number of bone fragments through CT images and 3D digital models, respectively. The latter were analysed in Geomagic Design X software to determine the biological profile of the individual. Various methodologies were taken into consideration and then selected based on the preserved diagnostic districts. To estimate the sex of the individual, the study performed by Cavazzuti et al. (2019) was used as reference. The preserved diagnostic traits (vertical diameter of the humeral head, maximum and minimum diameter of the humeral trochlea, maximum diameter of the radius head, vertical diameter of the femoral head) were independently measured, with the high-precision measuring tool available on the software, by two different observers in order to reduce inter-observer error (which was calculated by performing a Wilcoxon signed rank test). The measurement closest to the limit of 95% confidence interval – based on the relevant mean and standard deviation of cut-off values reported in Cavazzuti et al. (2019) – was then used for the determination.

Age at death was estimated through observation of the 3D surfaces of the anatomical elements at disposal. In particular, it combined the analysis of the level of epiphyseal closure (Buikstra and Ubelaker, 1994) and of the epiphyseal ring of the segmented vertebral bodies (Burns, 2015). As for the identification of pathological conditions, both CT images and 3D surfaces were observed by referring to the work of Ortner (2003).

4. Results

4.1. Traditional approach

4.1.1. Physical micro-excavation

The nine artificial cuts (photos in Appendix A) are described in Table 1. Each cut was composed of a clayey sediment whose colour transitioned from grey to brown as the excavation proceeded. A molten unguentarium, a second relatively well preserved unguentarium and a small overturned cup were recovered in layers 1, 2 and 3, respectively. Whereas, osseous fragments were recorded in every layer

4.1.2. Traditional anthropological analysis

The human remains are composed of 1043 fragments (Fig. 2), for a total weight of 1135.4 g. No recognisable anatomical element suggests the presence of more than one human individual; hence the tomb was considered as a single deposition.

On a general level, the sample appears to be fairly fragmented, since most of it (88% of fragments) measures less than 3 cm, while only 4% are larger than 4 cm (for further details see Appendix B). Due to the high degree of fragmentation, the majority of the elements (53%) could not be determined with accuracy and were therefore divided into: diaphyseal fragments (34%), epiphyseal fragments (5%), spongy bone fragments (3%) or indeterminates (11%). Conversely, the fragments for which a determination was indeed possible (47%), are mainly represented by: cranium (17%), ribs (6%), vertebrae (6%), femur (5%), humerus and pelvis (both 4%).

The bulk of the sample (84%) is ascribable to combustion phase 3, meaning it was exposed for a prolonged length of time to particularly

Table 1
Results from traditional micro-excavation of tomb 1, funerary area 2.

Layer n.	1	2	3	4	5	6	7	8	9
Layer h. (cm)	20	18	16	12	10	8	6	4	2
Layer d. (cm)	20	18	18	18	18	18	17	16	16
Layer colour	gray	grayish-brown	grayish-brown	grayish-brown	brown	brown	brown	brown	brown
Layer matrix	clay	clay	clay	clay	clay	clay	clay	clay	clay
Presence of bones	X	X	X	X	X	X	X	X	X
Presence of grave goods	molten unguentarium	unguentarium	small cup	/	/	/	/	/	/

Fig. 2. Osteological remains arranged by anatomical region.

high temperatures (ranging from 750/800 °C to over 1000 °C). Whereas 11% is ascribable to intermediate phase 2–3 and only 5% to phase 2. The initial combustion phases (1 and 1–2) are not present.

A limited 4% of the fragments are partly covered by concretion, mainly the ones attributed to phase 3 (3%). More frequent is the presence of iron oxides (21%), identified by reddish-brown marks on the bone surface (Dunlop, 1978; Dupras and Schultz, 2013; Fernández-Jalvo and Andrews, 2016). Also these are mainly present on phase 3 bones (16%).

Regarding the distribution pattern of the different skeletal elements in the urn, no evident order was observed. No body portion was predominant in any artificial layer, with the exception of layer 1 that presented exclusively few cranial, rib and diaphyseal fragments (for a total of 17 elements). Similarly, layer 2 also included a small number of fragments (n. 39) which were, however, more varied. Whereas layer 7 resulted as being the most abundant with 277 elements. Cranial portions and indeterminate diaphyseal elements are, instead, common throughout the near totality of the layers (for images representing the single layers, see Appendix C).

It was not possible to estimate sex. Whereas, the estimation of age at

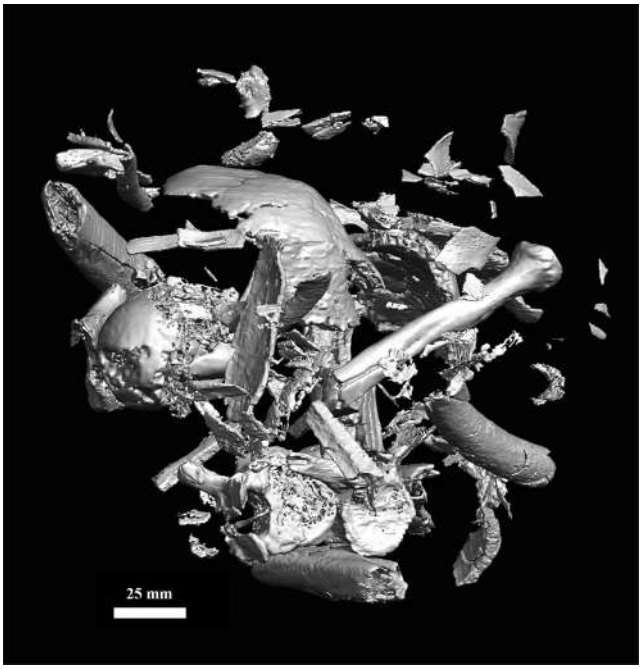

Fig. 3. Result of virtual micro-excavation (as positioned in the urn).

death was limited to the ascertainment of the skeletal maturity of the individual (≤ca. 50 years of age) through the observation of a conserved portion of the right auricular surface (Buikstra and Ubelaker, 1994) and of the right pubic symphysis (Brooks and Suchey, 1990). The only pathological condition that was observed is a Schmörl's node (Ortner, 2003) on the lower endplate of a vertebra from the middle thoracic portion. Moreover, some small bone spicules were detected on the body margin of a further thoracic vertebra and the fusion of a lower molar root was observed.

As far as the grave goods are concerned, in addition to the elements which were recognised and extracted during excavation (two glass unguentaria and a small cup), very small fragments of pottery (eight chips and one fragment of a lip) and 13 light blue, thin fragments of glass were recovered among 47 fragments of worked bone. Most of the latter (41 out of 47) presented distinct traces of processing, which was so heavy that determination was possible for only nine fragments, all from the diaphysis of a bovine radius. Moreover, it was also possible to recognise different types of striation: the more parallel, equally distanced and superficial ones – which are typical of sanding – and the deeper ones with intersecting striations – which are typical of a sawing movement (Symes et al., 2010).

Relevant, is the recovery of two fragments of a small bone plaque decorated with the profile of a human face. Moreover, a total of nine fragments presented regular and symmetrical notches on their long side. Conversely, the remaining six bone fragments that presented no trace of processing comprised four diaphyses of non-determinable mammals, a portion of a non-fused rib epiphysis of a young non-determinable mammal and what likely is a portion of a large-sized ungulate horn.

No particular distribution of non-human bones and of grave goods was discerned, though none were recovered from layer 8.

4.2. Virtual approach

Prior to segmentation, many elements could already be recognised by looking at the CT images: pottery (the urn, an overturned cup and some sparse fragments), a metal object (a modern-day nail used to keep the tag in place), grave goods (an unguentarium and 2 other molten glass elements), bones (in particular cranial, vertebral, diaphyseal and epiphyseal elements, just as various indistinct fragments).

This allowed the selection of 58 osseous elements to be manually segmented, whereas other 83 smaller and indeterminate fragments were segmented automatically (Fig. 3). Among the former, two fragments revealed a carved surface and were thus classified as osseous elements of the funerary bed. Consequently, other 16 small fragments that presented a similar morphological configuration (very thin and flat fragments of exclusively cortical bone) and a similar higher density – although did not present any signs of carving – were considered as possible further appliques of the funerary bed and hence classified as grave goods.

The remaining 40 segmented elements were all determined as human remains, none of which suggested the presence of more than one human individual. Since the segmentation was partial and non-arbitrary, statistical calculations regarding size, presence of specific characteristics and determinability of the sample were not performed.

Among the segmented human remains, there are 24 undetermined elements: nine diaphyseal portions (ranging from 3.7 to 9.5 cm of length) and fifteen utter indeterminates (all, except one, ≤ 3 cm of size). Conversely, 16 elements were determined: four generic cranial portions (all, except one, greater than 4 cm in size), a right temporal portion, a nearly integral occipital, the right mandibular ramus (missing the condyle), three vertebrae with different degrees of fragmentation, one rib fragment, the left humeral head with its surgical neck, the distal end of the left humerus, the proximal portion of the left radius, the right femoral head and neck, and the distal portion of a metatarsal.

As far as sex estimation is concerned, all the traits measured by either observer – although in some cases conservative due to the fragmentary condition of the elements – resulted in being higher than the pertaining limit of the confidence interval of the cut-off value reported in (Cavazzuti et al., 2019), with one exception: the maximum diameter of the humeral trochlea (Table 2). Moreover, results from the Wilcoxon signed ranked test ($V = 3$, p-value $= 0.3125$) indicated a consistency in the measurements taken by both observers. Hence, regardless of the discordance posed by the maximum diameter of the humeral trochlea, the individual was classified as male.

Age at death, based on the absence of any evident fusion line (Buikstra and Ubelaker, 1994) on the segmented anatomical elements and on the degree of osteophytic lipping on the vertebral body (Burns,

Table 2
Measurements of diagnostic traits for sex determination compared with mean cut-off points (Cavazzuti et al. 2019) and relative upper and lower limits of 95% CIs (listed according to accuracy level).

Trait	Accuracy (%)	Precision in male diagnosis (%)	Precision in female diagnosis (%)	Cut-off point (mm)	Confidence interval	Measurements taken by researcher 1 (mm)	Measurements taken by researcher 2 (mm)
Radius: head maximum diameter	88.3	88.1	88.5	18.32	18.28–18.36	20.48	20.60
Femur: vertical head diameter	81.3	82.7	80.2	39.42	39.21–39.63	40.21	40.45
Humerus: vertical head diameter	80.0	73.4	84.1	37.88	37.73–38.03	38.70	39.63
Humerus: trochlea maximum diameter	73.1	70.1	74.9	19.98	19.87–20.09	18.76	19.40
Humerus: trochlea minimum diameter	72.3	63.0	79.5	13.27	13.22–13.32	14.48	13.96

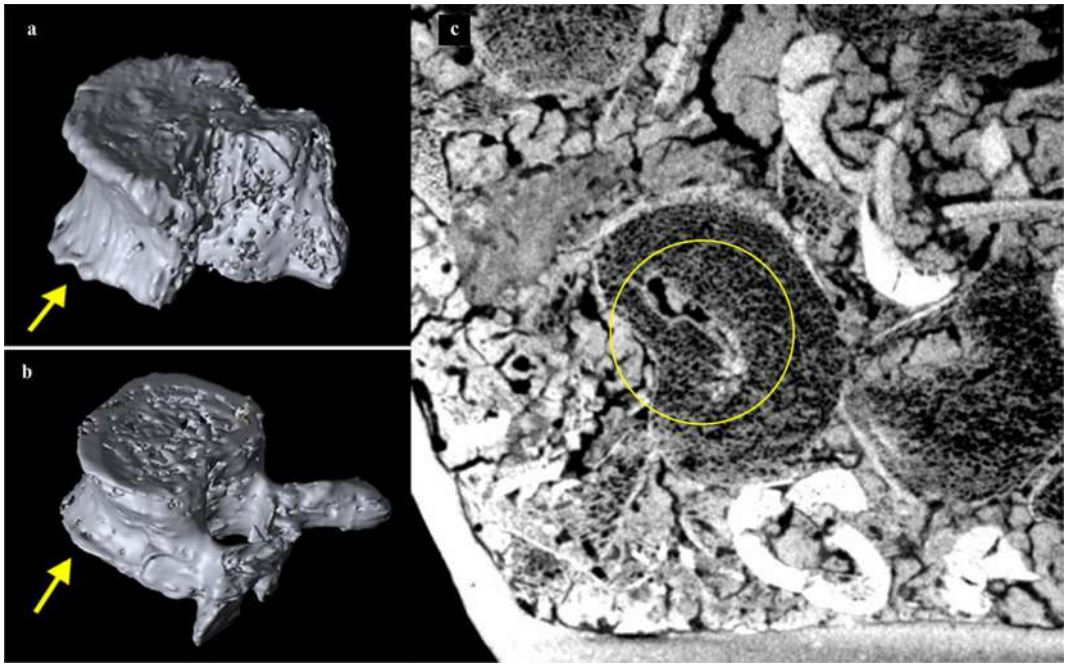

Fig. 4. a, b) Virtual models of the vertebrae presenting osteophytic lipping; b) Schmörl's node as seen from CT scan.

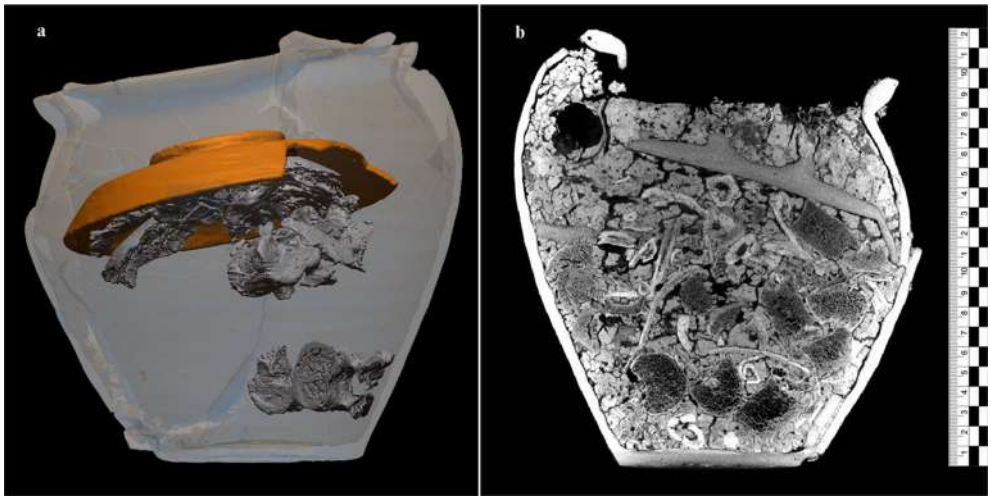

Fig. 5. Spatial distribution of: a) cranial and vertebral elements in 3D reconstruction; b) vertebral elements in CT image.

2015) of two of the segmented vertebrae (Fig. 4a), was estimated to be at least over 30 years. Besides, on a pathological level, a Schmörl's node (Ortner, 2003) was also identified through the CT images (Fig. 4b).

At this stage of the research, it was not possible to identify the combustion phases of the fragments, contrarily to bone fractures and modifications caused by said combustion that were distinctly visible on the cortical portions of the bones.

As far as the grave goods are concerned, three unguentaria (two molten and one essentially intact), an overturned ceramic cup and 18 funerary-bed bone fragments were segmented. Among the latter, two presented relief decorated surfaces. Moreover, some peculiar materials for shape and density were noticed in the CT images. The position of these elements was recorded, although only a few of the smaller elements were segmented. Among these: some very small spherical and hollow objects (≤ 3 mm of diameter) that present two holes on opposite sides; sparse, small, shiny grains that range between 0.6 and 1.3 mm of size that – due to the brightness at which they were rendered by the CT scan – were interpreted as possible iron oxide agglomerates.

Finally, as to the distribution pattern of the different elements within the urn, the majority and the more complete skeletal elements were visibly positioned below the overturned small cup, whereas the area above it offered a more barren appearance. Moreover, below said cup, certain anatomical districts appeared to be concentrated in specific areas of the urn: the cranial components were positioned directly under the cup (with the exception of few small fragments, which were further down) (Fig. 5a) and the vertebrae appeared to be concentrated on one side of the urn (Fig. 5a, b).

Contrarily, the segmented grave goods were mainly recorded either in the higher portion of the urn, in particular above the overturned cup, or along its sides. Notably, two out of three *unguentaria* were located in proximity to the top of the urn, whereas the third was positioned directly below, in correspondence with the collapsed edge of the

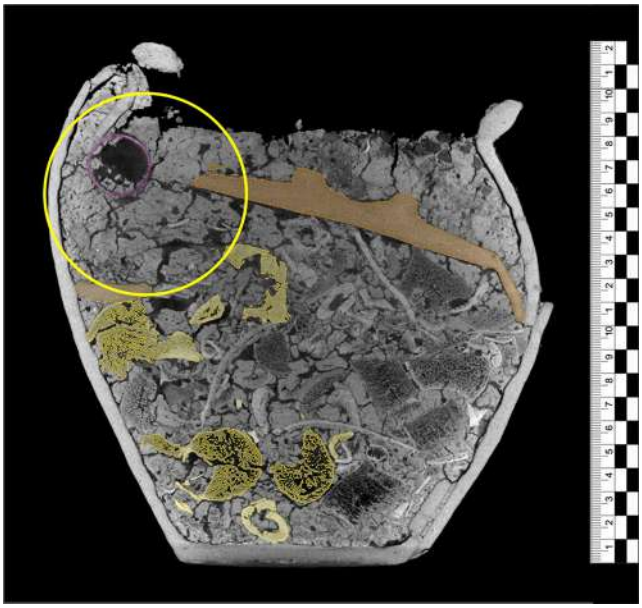

Fig. 6. CT image of the urn showing the accumulation of sediment (in yellow circle). Also in picture: the nearly intact unguentarium (in purple), the overturned cup and one of its broken fragments (in orange), and labelled bone elements (in yellow).

overturned cup and in proximity to the severed fragments of the latter. Moreover, in this same area, a conspicuous accumulation of sediment was observed from the CT images (Fig. 6).

5. Discussion

The degree of fragmentation that occurs during micro-excavation is apparent when comparing images and models from the virtual approach with the extracted remains of the traditional approach.

The substantial fragmentation caused by the traditional method, can depend on several factors: texture, hardness or dryness of the soil; the tools that are used or the skill of the person conducting the excavation; and the intensity at which the bones were originally cremated.

Since the more calcined elements present a higher resistance to mechanical and chemical stresses (Aplin et al., 2016; Harvig et al., 2012; Kalsbeek and Richter, 2006), it is not surprising that, in the traditional method, combustion phase 3 is by far the most represented. Whereas, elements presenting lower calcination and mineralisation – associated with the lower combustion phases – are remarkably scarce or absent. The low representation of such elements might not only be directly ascribed to the intensity of the cremation or to a selection of the bones during the cremation ritual, but might also be caused by their obliteration during excavation. Consequently, this might have led to a significant underestimation of the total volume and weight of the sample – partly accounting for the low value that was recorded in this study (1135.4 g) – and to an overestimation of the intensity of the cremation (Harvig et al., 2012).

Conversely, the employment of virtual micro-excavation allowed the preservation and observation of even the most brittle elements, providing more complete anatomical components. However, the virtual approach did not allow the identification of different combustion phases, hence it was not possible to verify the role assumed by this aspect in the fragmentation and obliteration of the anatomical elements. Moreover, the occurrence of such obliteration does not allow an unambiguous overall comparison of the degree of fragmentation – performed by comparing the total number and size of fragments – due to the consequential difference in the composition of the samples retrieved by the two methods. Regardless, due to the decision to focus the segmentation operation on the recognisable and most diagnostic elements – which led to the partial investigation of the sample in the virtual approach – this comparison would not have been in any case possible.

However, a full appreciation of the contrast in the degree of

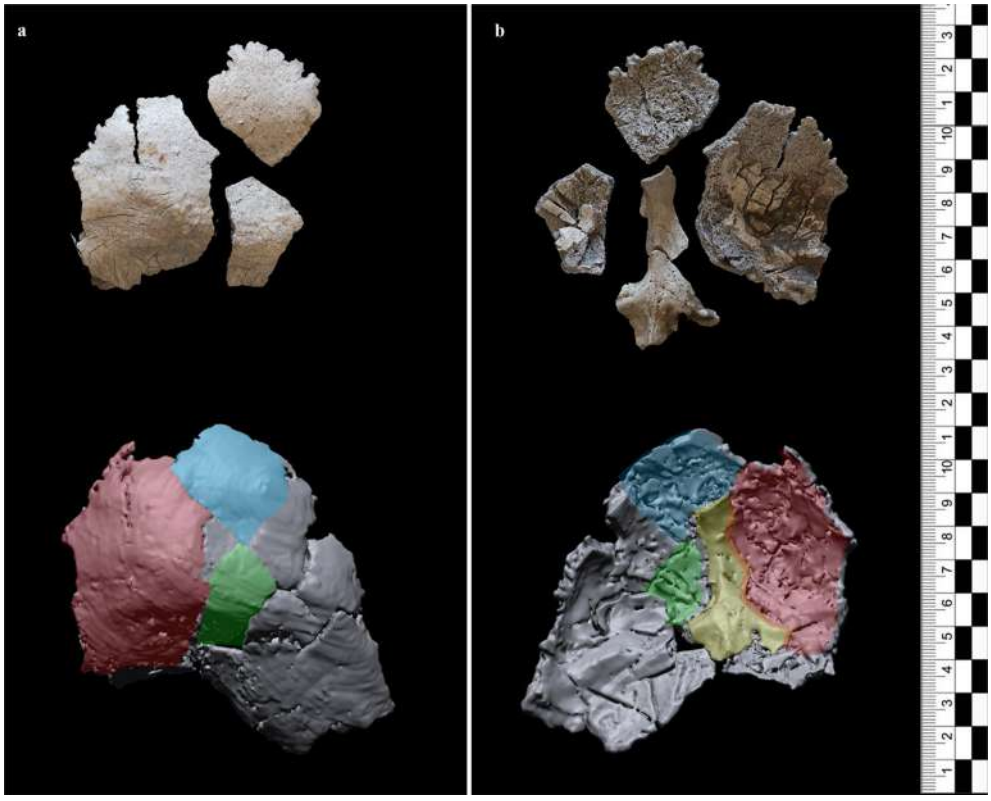

Fig. 7. Comparison between physical (top) and virtual (bottom) fragments of occipital: a) external view; b) internal view.

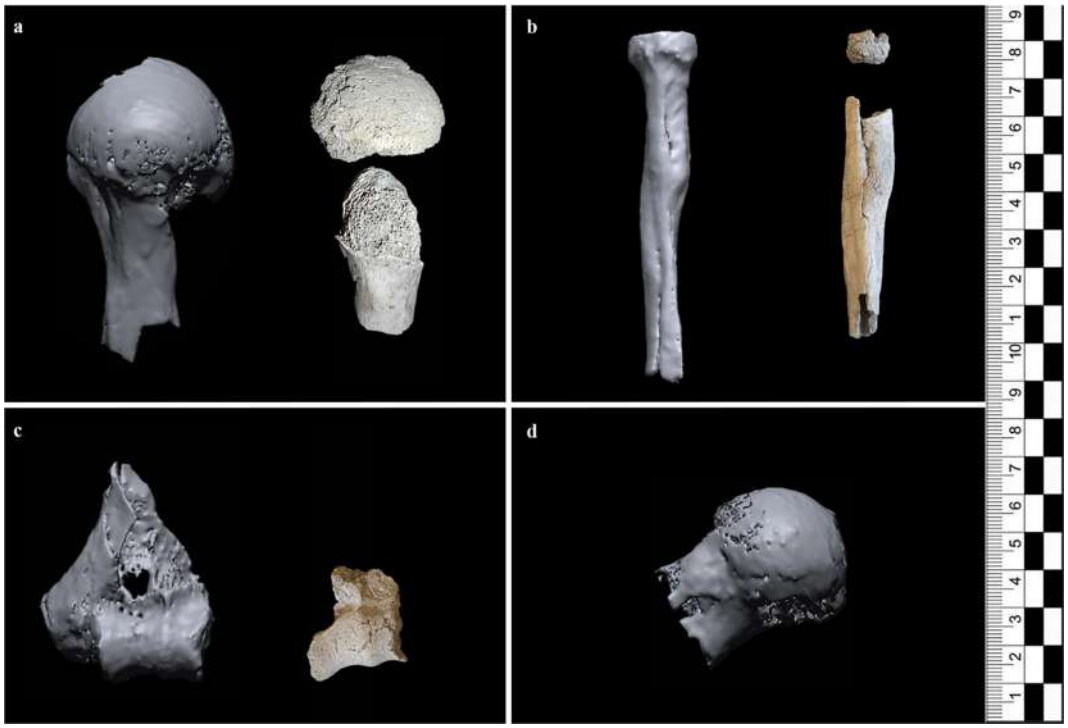

Fig. 8. Comparison between virtual (left) and physical (right) fragments of: a) proximal portion of left humerus; b) distal portion of left humerus; c) left radius; d) femoral head (the physical element was not retrieved).

fragmentation can still be achieved through the comparison of the condition in which single anatomical elements were recovered in either approach.

Representative is the case of the occipital, with the virtual approach being able to extract a large and more complete portion, whereas the traditional method recognised only three smaller joining fragments (Fig. 7).

Similarly, the virtual method also allowed the acquisition of diagnostic sections of various anatomical elements, whereas the traditional method was only able to retrieve some recognisable – though non-diagnostic – fragments. In particular, the proximal and distal portions of the left humerus (Fig. 8a, b) and the proximal portion of the left radius (Fig. 8c) were recovered intact through the virtual method, whereas the traditional method retrieved smaller and fragmentary elements.

Ultimately, the case of the femoral head perfectly demonstrates how the virtual approach allows the preservation, recovery and – if diagnostic – measurement of certain anatomical portions that the traditional method might disintegrate. In this case, no discernible fragment of the femoral head was recovered in the traditional approach (Fig. 8d).

The higher degree of preservation assured by the virtual approach ultimately allowed the estimation of the individual's sex (male). This same estimation was not possible through the traditional approach due to the excessive fragmentation of the remains and to the obliteration of the diagnostic traits. As far as estimation of age at death is concerned, since it is usually based on a morphological – rather than metrical – analysis, the absence of the original bone texture may add some minor disadvantage. Nonetheless, the higher level of preservation and integrity ensured by the virtual approach, although regarding a limited selection of the sample, has presented a greater number of observable traits (e.g. presence/absence of fusion lines) that have allowed a more effective estimation.

Whilst the only identified pathological feature – detected in either approach – was a Schmörl's node on a middle-thoracic vertebra. In the virtual approach, its presence was clear in the CT images (Fig. 4b).

Moreover, the virtual approach does allow the observation of context and bones before disturbance, giving information regarding the

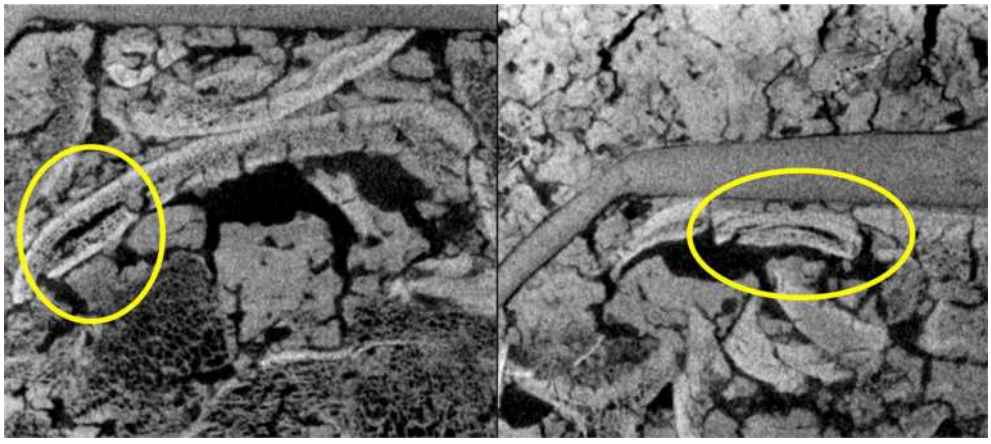

Fig. 9. Examples of delamination from CT scan: details of occipital (left) and of parietal (right).

Fig. 10. Comparison among virtual (left) and physical (right) decorated funerary bed plaque.

progression of different types of heat-induced bone modifications. In particular, the delamination of cranial elements that was observed in the traditional method, was documented still in its incipient stages in the CT images used for the virtual approach (Fig. 9).

Conversely, the traditional approach might result in being more effective in the identification of concretions, iron oxides and striations on the bone surfaces, since the virtual method did not record any. The first would certainly have shown in the CT images, though it either was not included in the segmentation of the bone because too similar to the hardened clay, or it was expunged during the surface optimisation of the bone's 3D model. Whereas, regarding the presence of iron oxides, the virtual approach did not detect it on the bones, though small shiny grains were recorded throughout the sediment. These grains, due to their size and rendered luminosity were interpreted as agglomerates of iron oxide. Regardless of the reliability of such interpretation, since the traditional method did not detect the presence of such elements, their sole identification is further confirmation of the support virtual technology can provide towards a thorough documentation. As far as striations on bone surfaces are concerned, the virtual approach did not register any. At the time being, it would not appear possible to document them with the scanning detail used for the investigation of an overall urn, whereas it is known to be possible in the examination of elements scanned with micro-CT (Norman et al., 2018).

The virtual approach has also demonstrated to be an excellent resource in the identification and study of artefacts. Although this aspect has not been closely pursued in this study, the high degree of preservation insured by such approach allowed the observation of the grave goods in as integral a state as possible (e.g. the plaque decorated with the profile of a human face, extracted in two separate fragments by the traditional method, was recovered in one piece by the virtual approach: Fig. 10) and the detection of elements which were not recovered nor documented in the traditional method (e.g. a third molten *unguentarium*, a second carved bone fragment and small, hollow spherical objects of unknown material: Fig. 11).

Although unanticipated materials may be challenging to identify, the possibility to investigate the interior of the elements supplies a further instrument for the recognition and for an in-depth analysis of the objects, which would otherwise be impossible without damaging the artefact. Moreover, the ability to detect specific elements and their exact location within the context allowed by the virtual approach, also enables targeted sampling in the traditional method, so as to compromise the contents as little as possible. This aspect may be important since a guided and targeted sampling would allow the recovery, preservation and identification of those peculiar elements that are often missed by random sampling and then destroyed by excavation.

Ultimately, the virtual approach is also able to deliver a deepened and enhanced analysis of the distribution pattern. Due to the subdivision in artificial layers at which the traditional approach is limited, research has regularly focused on the cremated remains alone, studying them independently from their original archaeological and geological context (Harvig et al., 2012). With the 3D recreation of the urn and its contents, it is possible to have a comprehensive view of the context or to isolate and manipulate specific elements in order to observe them from the best viewpoint possible.

As an example, in this study the traditional approach was not capable of distinguishing particular distribution patterns of either anatomical elements or grave goods, whereas the virtual approach – despite it being a preliminary analysis – was able to recognise different pattern distributions for either class of elements. It recorded a large concentration of vertebrae in one half of the urn and a cluster composed of the majority and more voluminous cranial fragments positioned at the top of the heap of bones, thus indicating a certain level of organization of the deposition. Moreover, it also recorded the location of the segmented grave goods, which all resulted in being either in the higher, more barren portion of the urn or along its sides. In particular, the disposition of the *unguentaria* reveals how at least two of them must have been deposited above the overturned cup and an infiltration of sediment, fracturing the overturned cup, allowed some elements (i.e. the non-molten *unguentarium*) to breach into the lower part of the urn. Such interpretation is supported by an accumulation of soil in correspondence with the fracture, with very few small bone fragments and the non-molten *unguentarium* encased in it, and the ceramic shreds of the cup directly below it (Fig. 6).

The biggest problem that was encountered in the application of the virtual approach to the study of an archaeological context was time expenditure, closely followed by the highly specialised and expensive equipment which was needed. The high expenditure of time was caused by the impossibility to proceed with automatic segmentation due to the lack of sufficient contrast between different materials on two different scales. On an extended scale, lack of contrast could be presumably attributed to the exsiccation process that the different elements underwent during the long period elapsed between discovery and scanning. This most likely caused the different materials to assume similar density levels, which translated in the generation of voxels of similar luminosities that are not easily distinguished by the automatic segmentation tool (global thresholding). However, there are many potential solutions to this problem: e.g. carrying out a timely scanning of the context; rehydrating the context; adjusting the scanning parameters. On the other hand, on a more localised scale, a further gradual loss in contrast was noticed as the rays advanced towards the centre of the scanned deposit. This can be attributed to the progressive loss of intensity of the X-rays as they are absorbed by the different materials they penetrate: a phenomenon called beam hardening (Fig. 12). This process causes the denser materials in the central area of the urn to be displayed with the same luminosity values as the less dense materials (such as sediment) at its

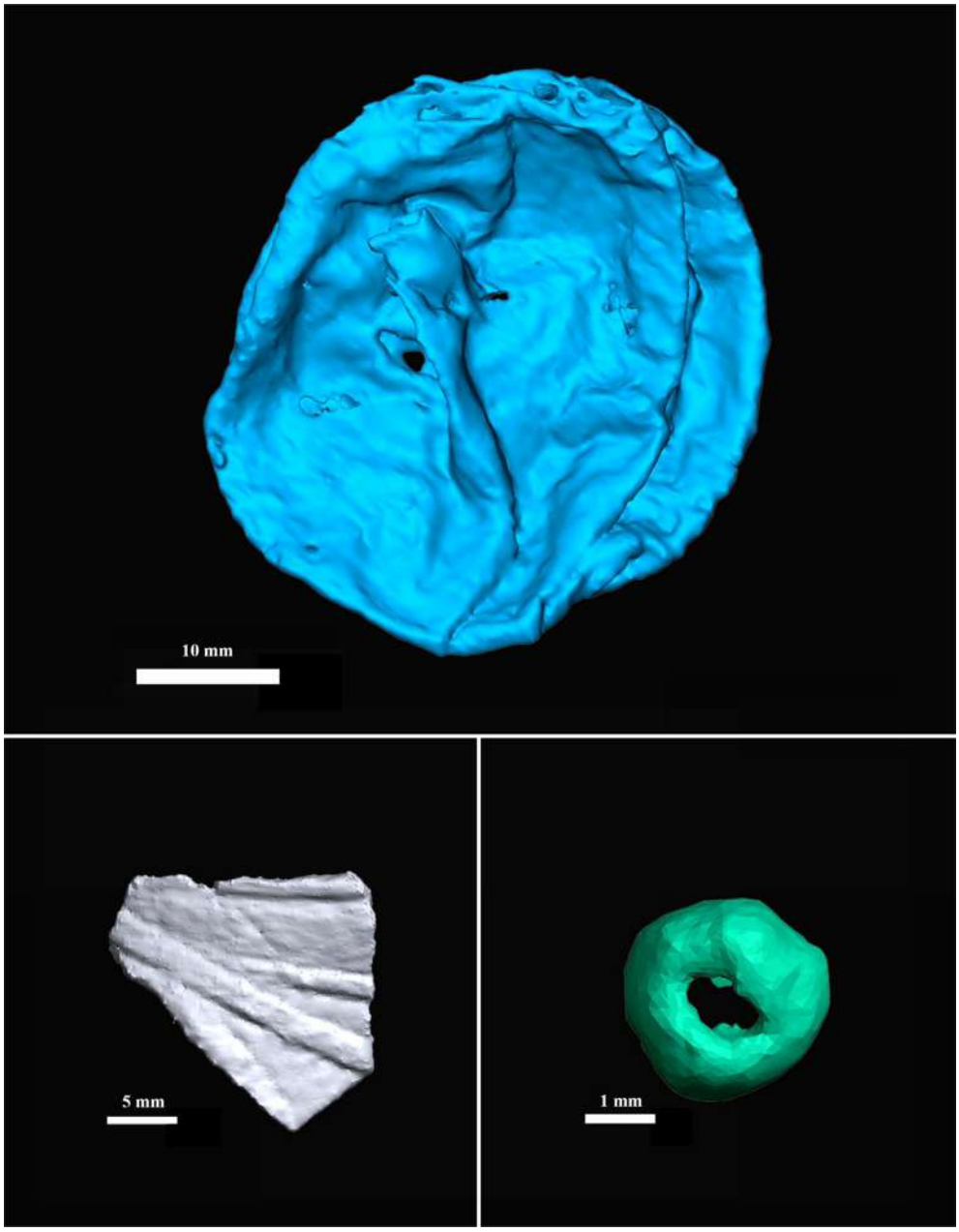

Fig. 11. Elements which were not detected by the traditional method: a molten unguentarium (top), a carved applique of the funerary bed (bottom left), a spherical object (bottom right).

margins, not allowing a uniform automatic segmentation throughout the urn. Also in this case, different methods have already been devised in order to reduce or correct the beam hardening effect (Brooks and Di Chiro, 1976; Hsieh et al., 2000; Kyriakou et al., 2010; Van Gompel et al., 2011).

6. Conclusions

The virtual micro-excavation has proved to be a promising technique for the investigation of archaeological contexts and, in the specific, of cremated remains. Not only does it favour the preservation of both context and remains, but it also allows a more complete and accurate documentation. Moreover, it is evident how, even on account of a preliminary analysis, the obtainable results are remarkable and ~~overly~~ exceed what was obtained by the application of the traditional method. The advantages regarding the mere analysis range from the possibility to observe context and sample as close as possible to their original condition, to a minor fragmentation and a more effective determination of both anatomical elements and biological profile, to a heightened and more accurate documentation and to a more incisive and global spatial distribution analysis.

The advantages are not limited to the archaeological and anthropological analysis and permeate to the restoration and musealization domains. These aspects were not examined in this study, though the possibilities are many: i.e. virtual restoration or support to traditional restoration; interactivity for the general public; simultaneous and widespread exhibition of the same materials; reduction of transport and insurance expenses (e.g. Urcia et al., 2018). Furthermore, it allows the simultaneous cooperation between different and distant teams and Institutions.

However, some limitations have been detected: the inability to perform chemical or pollinic analysis, the impossibility to observe chromatic differences, beam hardening effect, the need for highly specialised equipment and time expenditure. Although most of these can already be overcome with appropriate strategies and instruments.

A further concern might regard the reliability of the segmented surfaces. In this regard, as the technique develops and spreads, it

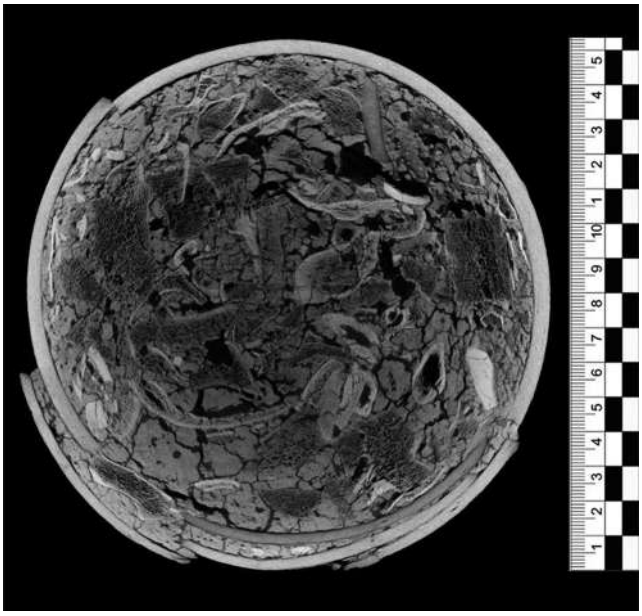

Fig. 12. Example of Beam hardening, with the central area of the scanned urn being darker than the outer.

certainly will be possible to devise explicit segmentation criteria to ensure both inter- and intra-transcriber consistency. The further development of this technique will surely encourage the surfacing of new procedures, applications and technologies, continuing to revolutionize the archaeological investigation process and to improve the data acquisition mechanism, giving access to new insight by allowing the acquisition of previously elusive – if not unattainable – information.

In this regard, possible next steps surely include the application of this approach to a variety of different contexts and materials to ensure its feasibility in diverse conditions and, as technology advances, with more extended contexts. As far as cinerary urns are concerned, the use of weight as sex indicator for cremated remains might be finally surpassed, it not being necessary anymore.

At the time being, although the virtual approach may be used in support of the traditional method, it has proved to already be a viable alternative to it. As the emerging technologies develop and become easily accessible – opening the road to automatic or deep learning segmentation methods and allowing a complete and thorough analysis in even less time and with less effort than with the traditional method – this new cutting-edge approach will predictably become the standard, taking a decisive step forward towards transcending the destructiveness of the archaeological discipline.

CRediT authorship contribution statement

Owen Alexander Higgins: Conceptualization, Methodology, Investigation, Data curation, Writing - original draft, Writing - review & editing, Visualization. **Antonino Vazzana:** Conceptualization, Methodology, Investigation, Data curation, Writing - original draft, Writing - review & editing, Visualization. **Lucia Martina Scalise:** Investigation, Writing - review & editing. **Federica Maria Riso:** Investigation, Writing - review & editing. **Laura Buti:** Writing - review & editing. **Sara Conti:** Data curation, Writing - review & editing. **Eugenio Bortolini:** Formal analysis, Writing - review & editing. **Gregorio Oxilia:** Writing - review & editing. **Stefano Benazzi:** Conceptualization, Resources, Writing - review & editing, Supervision, Project administration, Funding acquisition.

Acknowledgements

The authors acknowledge the contribution of Eurotec-lab for the support in the CT scanning of the urn. This research was conducted within the framework of the “Le necropoli romane di Mutina” project, promoted and coordinated by ‘Musei Civici di Modena’ (in the person of Silvia Pellegrini) and ‘Soprintendenza Archeologia, Belle Arti e Paesaggio per la Città Metropolitana di Bologna e le province di Modena Reggio Emilia e Ferrara’ (in the person of Cinzia Cavallari).

Appendix A

Phases of the traditional micro-excavation.
Figs. A1–A10.

Fig. A1. Top of layer 1.

Fig. A2. Top of layer 2.

Fig. A3. Top of layer 3.

Fig. A4. Top of layer 4.

Fig. A5. Top of layer 5.

Fig. A6. Top of layer 6.

Fig. A7. Top of layer 7.

Fig. A8. Top of layer 8.

Fig. A9. Top of layer 9.

Fig. A10. Emptied urn.

Appendix B

Representation of the degree of fragmentation of the anatomical elements in the urn. Seen divided per combustion phase (P1, P2, P3) or in their totality (purple bar).

Fig. B1

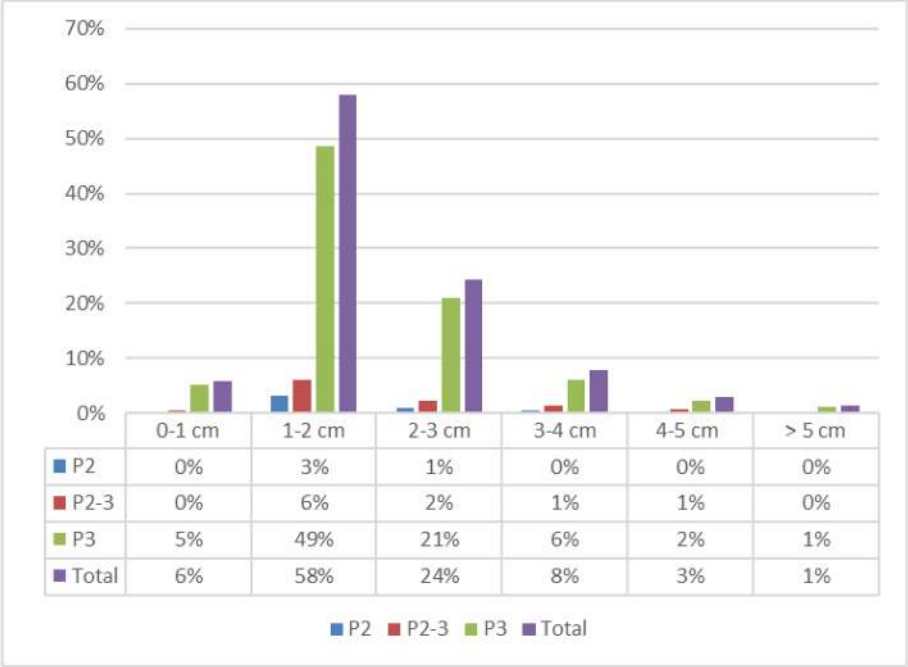

	0-1 cm	1-2 cm	2-3 cm	3-4 cm	4-5 cm	> 5 cm
P2	0%	3%	1%	0%	0%	0%
P2-3	0%	6%	2%	1%	1%	0%
P3	5%	49%	21%	6%	2%	1%
Total	6%	58%	24%	8%	3%	1%

Fig. B1.

Appendix C

Contents of urn divided per layer.
Figs. C1–C9.

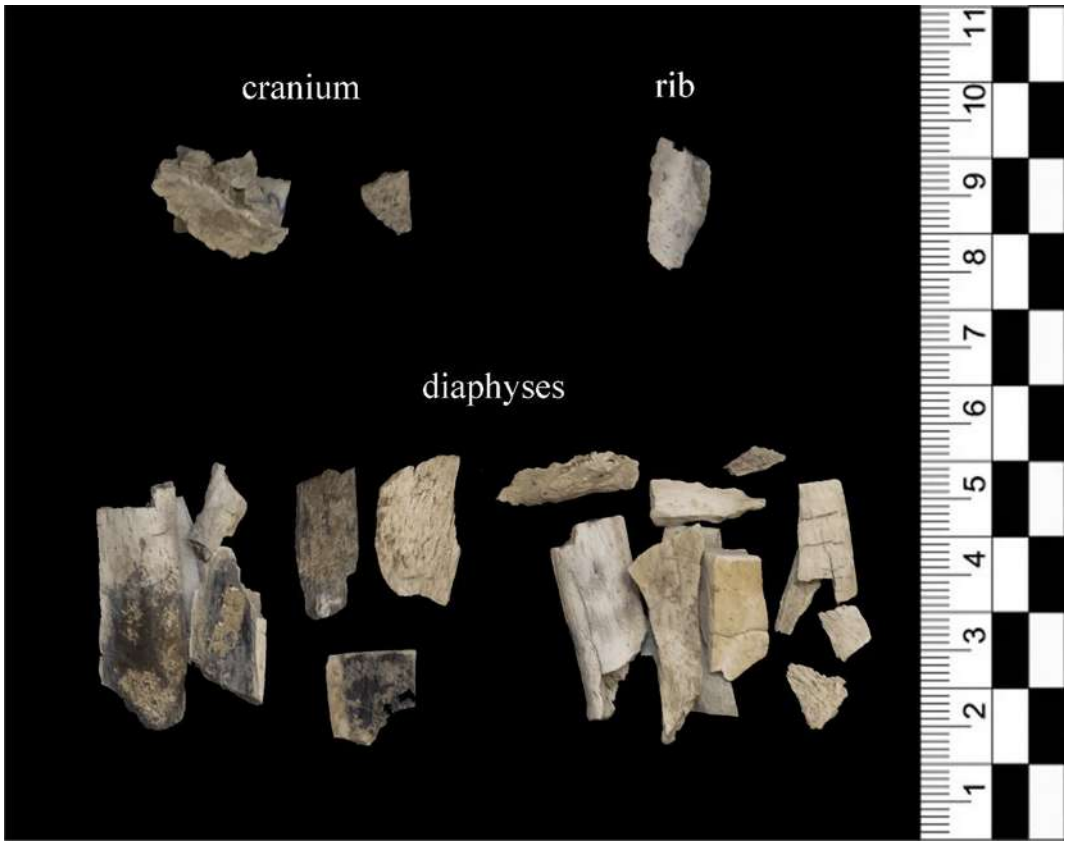

Fig. C1. Contents of layer 1.

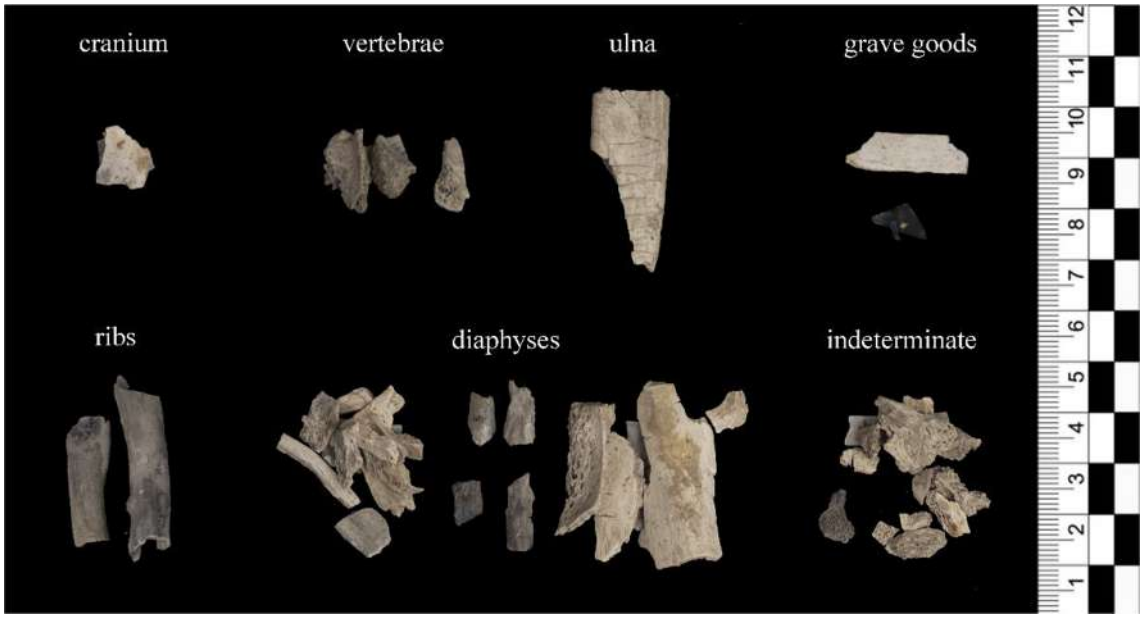

Fig. C2. Contents of layer 2.

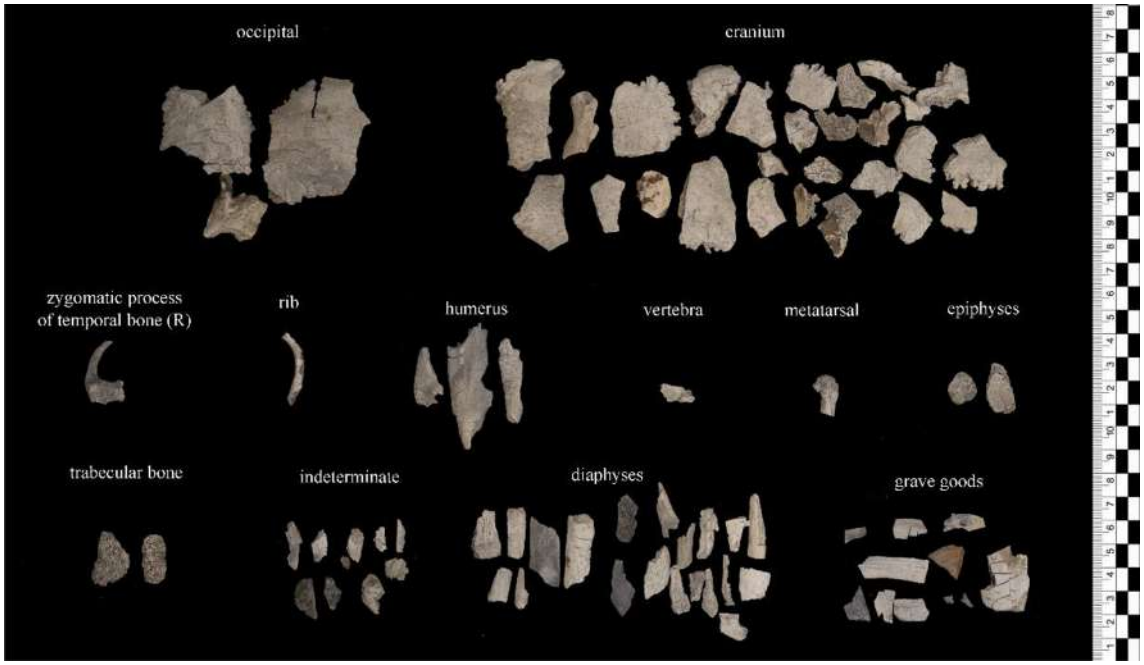

Fig. C3. Contents of layer 3.

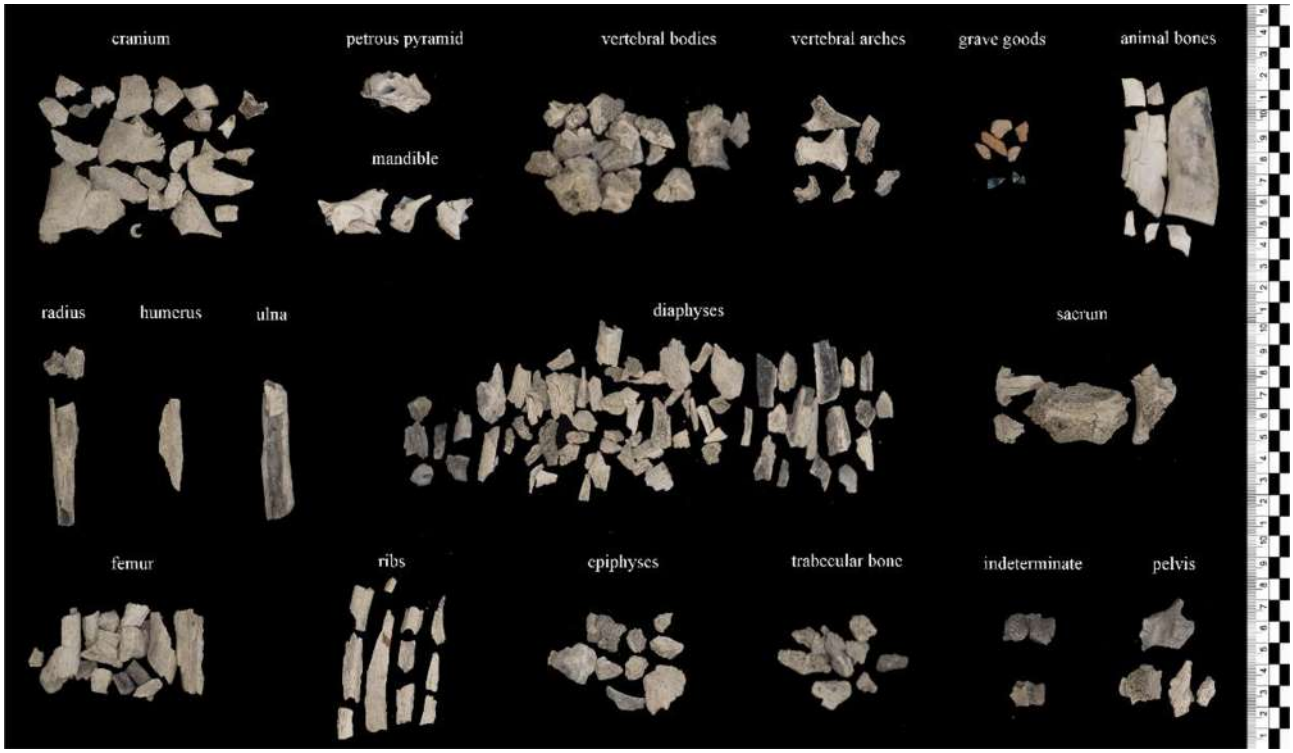

Fig. C4. Contents of layer 4.

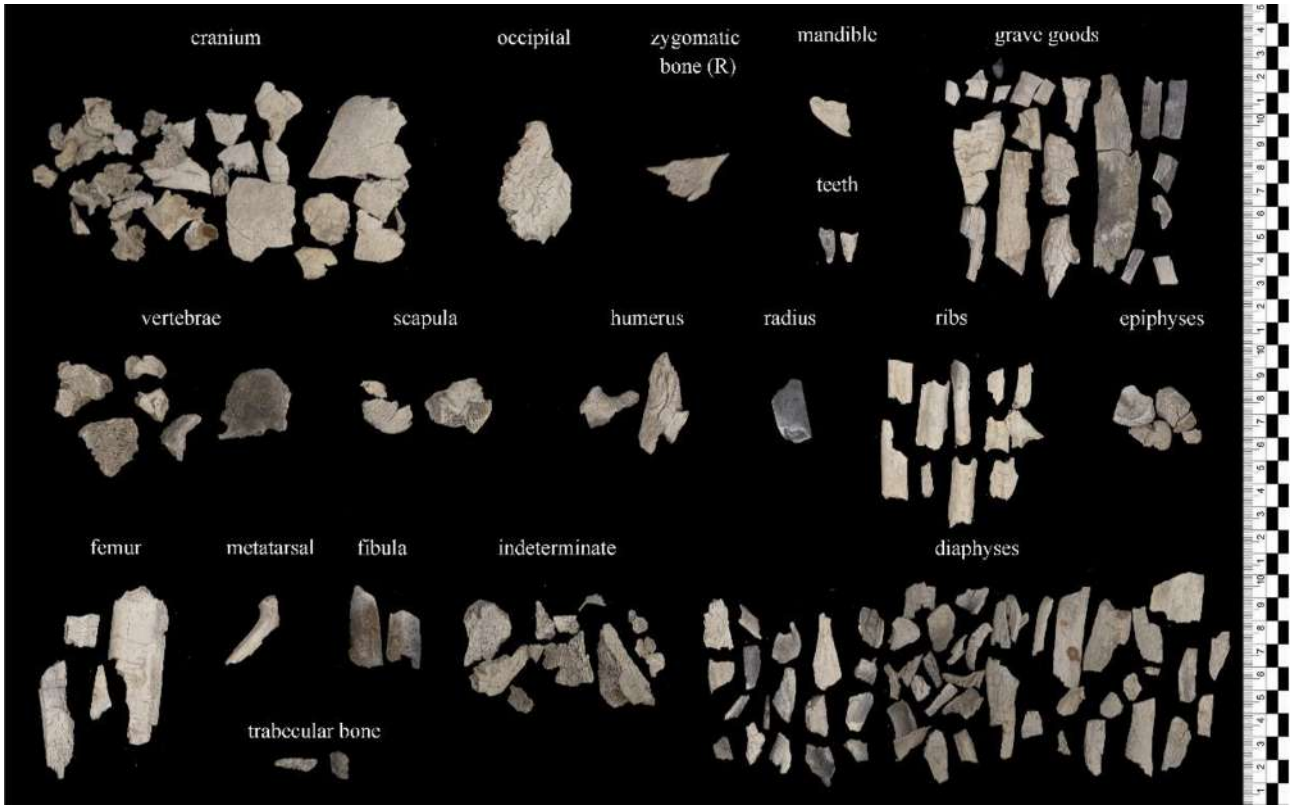

Fig. C5. Contents of layer 5.

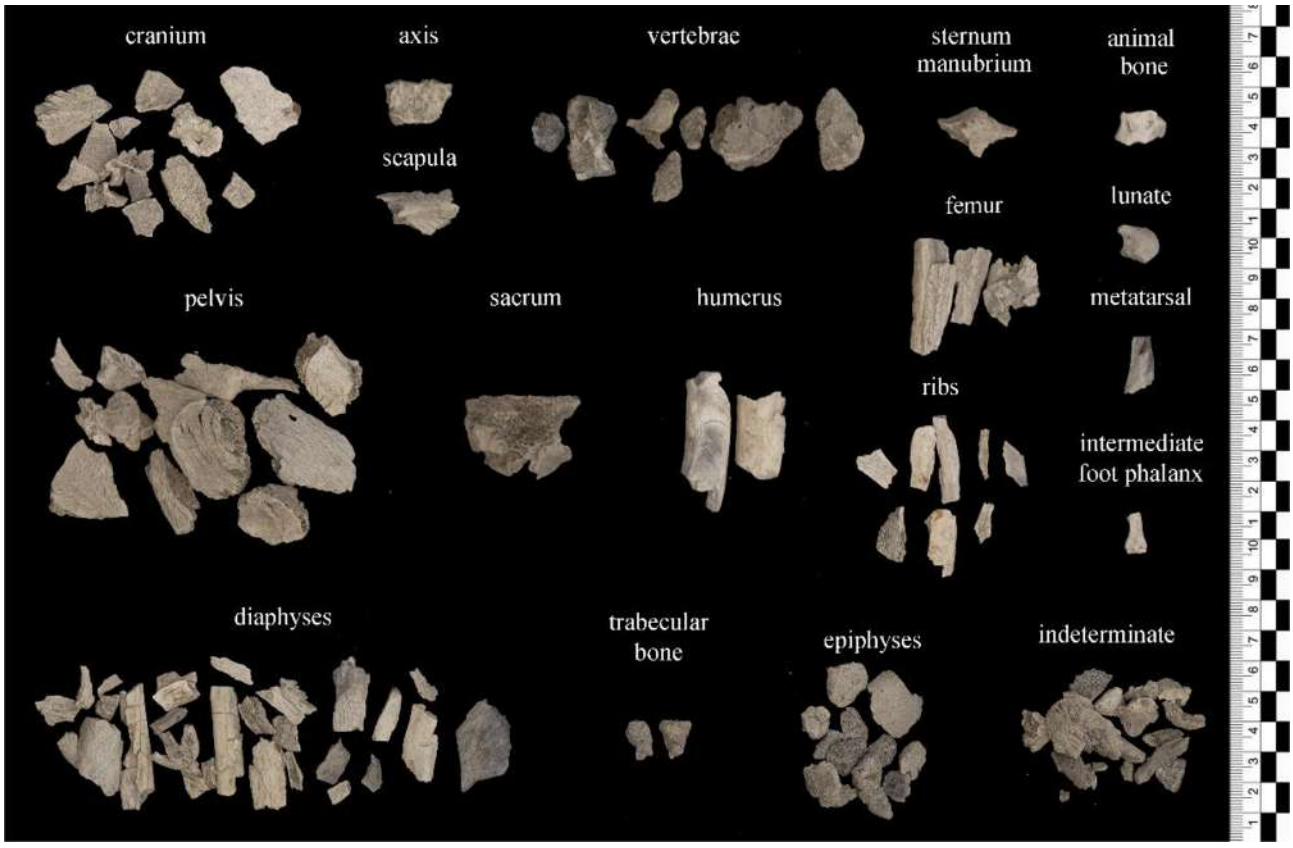

Fig. C6. Contents of layer 6.

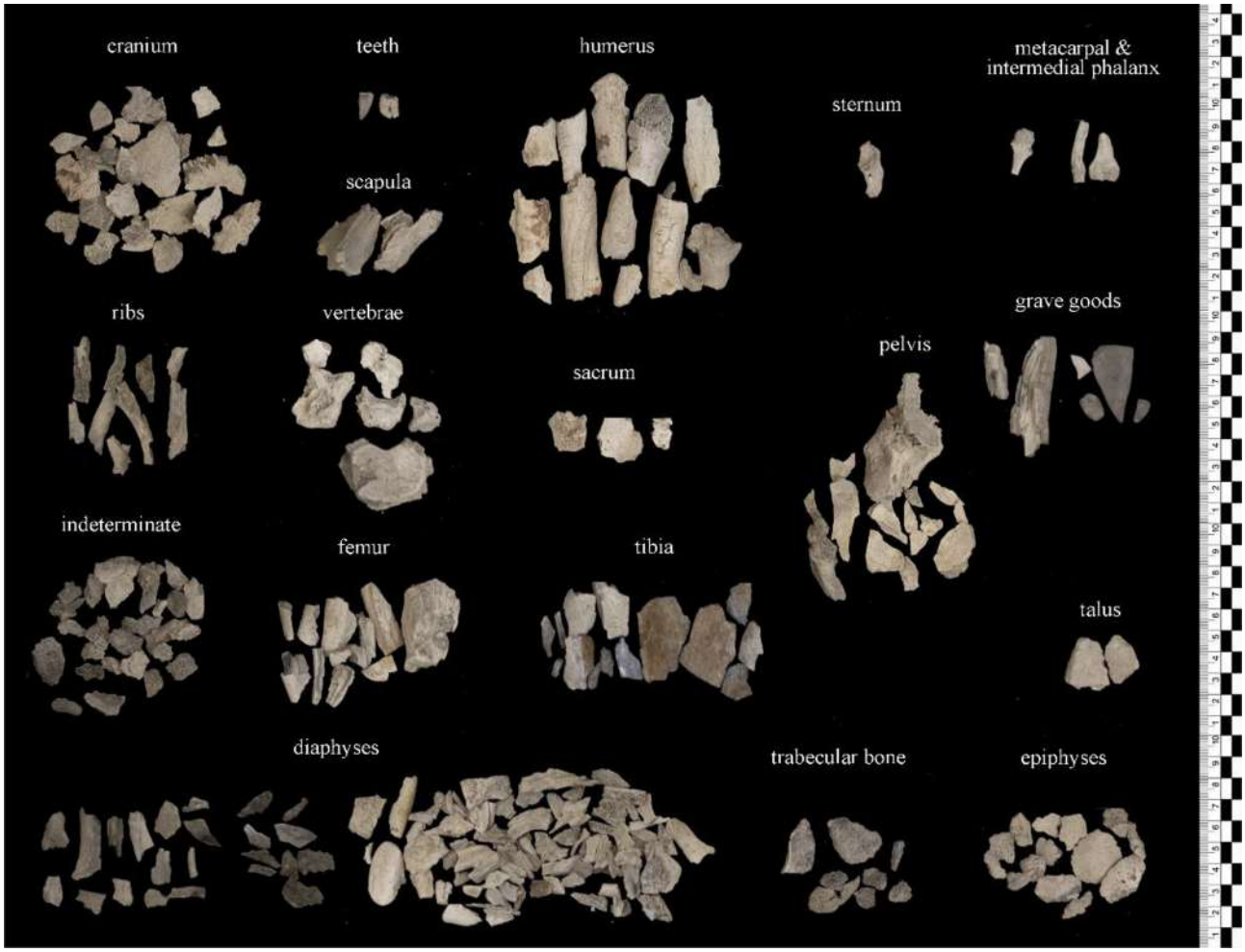

Fig. C7. Contents of layer 7.

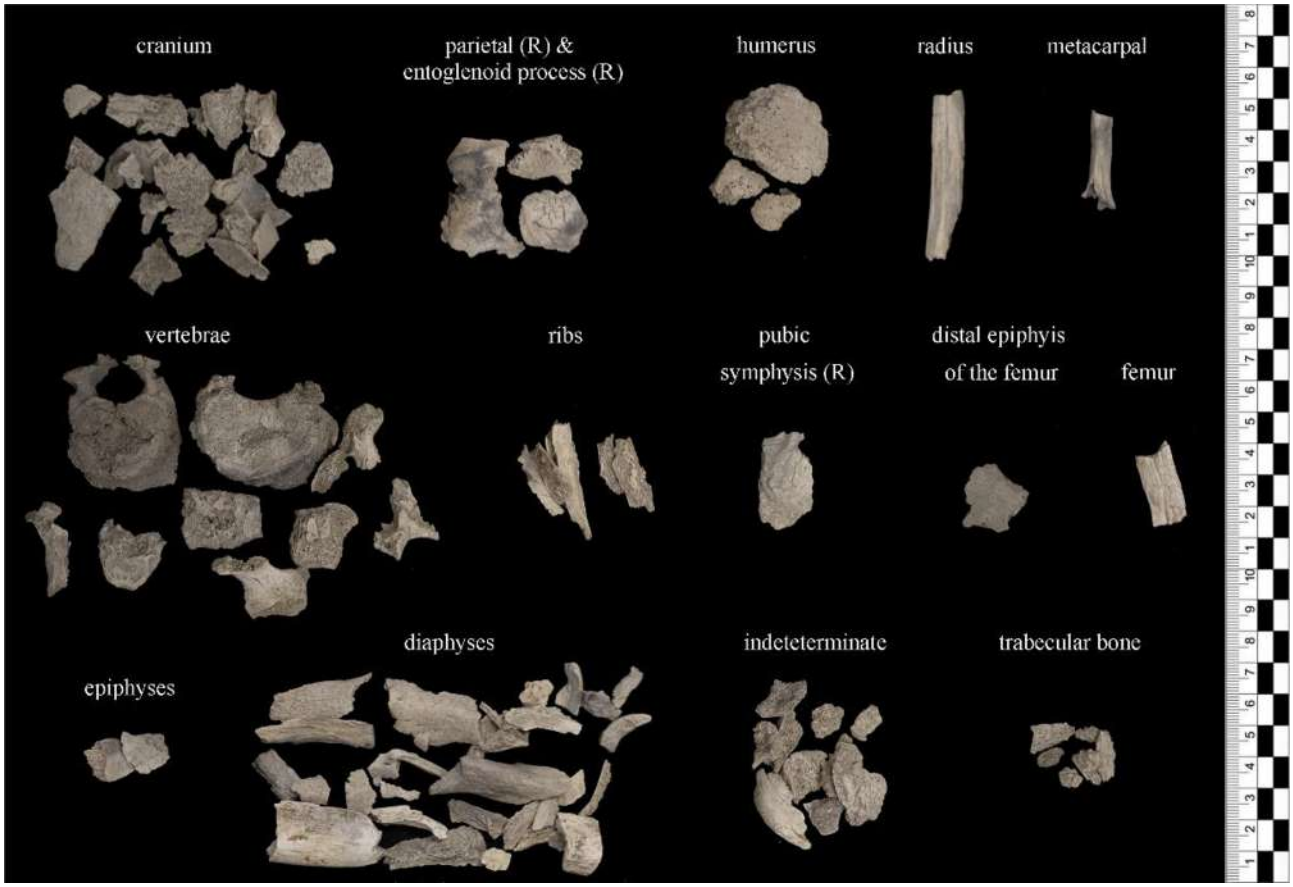

Fig. C8. Contents of layer 8.

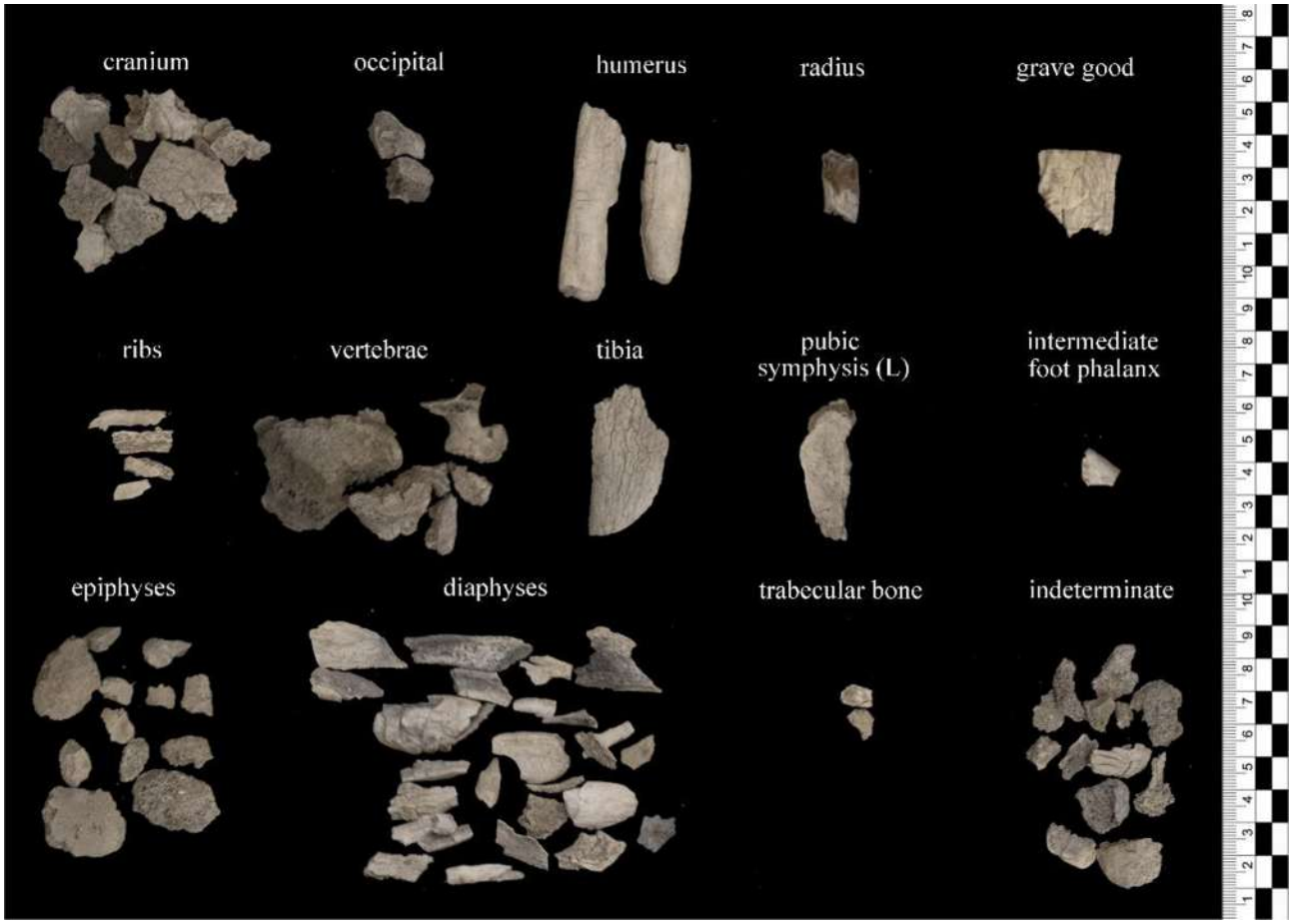

Fig. C9. Contents of layer 9.

References

Acsadi, G.I., Nemeskeri, J., 1974. History of Human Life Span and Mortality. Gy. Acsadi. J. Nemeskeri. Curr. Anthropol. 15, 495–507. https://doi.org/10.1086/201508.

Anderson, T., Fell, C., 1995. Analysis of roman cremation vessels by computerized tomography. J. Archaeol. Sci. 22, 609–617. https://doi.org/10.1016/S0305-4403(95)80146-4.

Aplin, K., Manne, T., Attenbrow, V., 2016. Using a 3-stage burning categorization to assess post-depositional degradation of archaeofaunal assemblages: Some observations based on multiple prehistoric sites in Australasia. J. Archaeol. Sci. Reports 7, 700–714. https://doi.org/10.1016/j.jasrep.2015.11.029.

Benazzi, S., Nguyen, H.N., Kullmer, O., Hublin, J.J., 2015. Exploring the biomechanics of taurodontism. J. Anat. 226, 180–188. https://doi.org/10.1111/joa.12260.

Benazzi, S., Nguyen, H.N., Kullmer, O., Kupczik, K., 2016. Dynamic modelling of tooth deformation using occlusal kinematics and finite element analysis. PLoS One 11, 1–17. https://doi.org/10.1371/journal.pone.0152663.

Brooks, R.A., Di Chiro, G., 1976. Beam hardening in X-ray reconstructive tomography. Phys. Med. Biol. 21, 390–398. https://doi.org/10.1088/0031-9155/21/3/004.

Brooks, S., Suchey, J.M., 1990. Skeletal age determination based on the os pubis: A comparison of the Acsádi-Nemeskéri and Suchey-Brooks methods. Hum. Evol. 5, 227–238. https://doi.org/10.1007/BF02437238.

Buikstra, J.E., Ubelaker, D.H., 1994. Standards for Data Collection from Human Skeletal Remains: Proceedings of a Seminar at the Field Museum of Natural History (Arkansas Archeological Report Research Series), in: Jonatha, H., Buikstra, J.E., Ubelaker, D.H., Aftandilian, D. (Eds.), Proceedings of a Seminar at the Field Museum of Natural History. Arkansas Archeological Survey, p. 218.

Burns, K.R., 2015. Forensic Anthropology Training Manual, Forensic Anthropology Training Manual. Prentice Hall. https://doi.org/10.4324/9781315664163.

Casu, S., Cagnini, A., 2016. TRA SCAVO ARCHEOLOGICO E RESTAURO. IL MICROSCAVO DEI MANUFATTI METALLICI DELLA TOMBA DI RADICONDOLI (SAN PIERO A SIEVE – FIRENZE)., in: XIV Congresso Nazionale IGIIC – Lo Stato Dell'Arte – Accademia Di Belle Arti Di L'Aquila – L'Aquila 20/22 Ottobre 2016. L'Aquila, pp. 1–7.

Cavalli, F., Innocenti, D., Cresnar, M., Vinazza, M., 2015. Multidetector computed tomography and micro-excavation of prehistoric urn from Novine / Hoarachkogel (Slovenia / Austria). Archäologische Biogr. einer Landschaft an der steirisch-slowenischen Grenze 238–244.

Cavazzuti, C., Bresadola, B., d'Innocenzo, C., Interlando, S., Sperduti, A., 2019. Towards a new osteometric method for sexing ancient cremated human remains. Analysis of Late Bronze Age and Iron Age samples from Italy with gendered grave goods. PLoS One 14, 1–21. https://doi.org/10.1371/journal.pone.0209423.

Cavazzuti, C., Salvadei, L., 2014. I resti umani cremati dalla necropoli di Casinalbo, in: Cardarelli, A. (Ed.), La Necropoli Della Terramara Di Casinalbo. Giglio Edizioni, pp. 669–708.

Chityala, R., Pudipeddi, S., Arensten, L., Hui, S., 2013. Segmentation and visualization of a large, high-resolution micro-ct data of mice. J. Digit. Imaging 26, 302–308. https://doi.org/10.1007/s10278-012-9498-y.

Dunlop, J.M., 1978. Traffic light Discoloration in Cremated Bones. Med. Sci. Law 18, 163–173. https://doi.org/10.1177/002580247801800304.

Dupras, T., Schultz, J., 2013. Taphonomic Bone Staining and Color Changes in Forensic Contexts, in: Pokines, J., Symes, S. (Eds.), Manual of Forensic Taphonomy. pp. 315–340. https://doi.org/10.1201/b15424-13.

Fernández-Jalvo, Y., Andrews, P., 2016. Discoloration and staining. Vertebrate Paleobiol. Paleoanthropol. 155–166. https://doi.org/10.1007/978-94-017-7432-1_5.

France, D., 2010. Human and Nonhuman Bone Identification, Human and Nonhuman Bone Identification. CRC Press. https://doi.org/10.1201/b10400.

Godinho, R.M., O'Higgins, P., 2017. Virtual Reconstruction of Cranial Remains: The H. Heidelbergensis, Kabwe 1 Fossil. Hum. Remain. Another Dimens. Appl. Imaging to Study Hum. Remain. 136–147. https://doi.org/10.1016/B978-0-12-804602-9.00011-4.

Gonçalves, D., Cunha, E., Thompson, T.J.U., 2013. Weight references for burned human skeletal remains from portuguese samples. J. Forensic. Sci. 58, 1134–1140. https://doi.org/10.1111/1556-4029.12167.

Hamilton, S.J., Green, M.A., 2017. Gross Post-Mortem Changes in the Human Body, in: Taphonomy of Human Remains: Forensic Analysis of the Dead and the Depositional Environment. John Wiley & Sons, Ltd, pp. 9–25. https://doi.org/10.1002/9781118953358.ch1.

Harvig, L., Lynnerup, N., Ebsen, J.A., 2012. Computed tomography and computed radiography of late bronze age cremation urns from denmark: An interdisciplinary attempt to develop methods applied in bioarchaeological cremation research. Archaeometry 54, 369–387. https://doi.org/10.1111/j.1475-4754.2011.00629.x.

Hsieh, J., Molthen, R.C., Dawson, C.A., Johnson, R.H., 2000. An iterative approach to the beam hardening correction in cone beam CT. Med. Phys. 27, 23–29. https://doi.org/10.1118/1.598853.

Kalsbeek, N., Richter, J., 2006. Preservation of burned bones: An investigation of the effects of temperature and pH on hardness. Stud. Conserv. 51, 123–138. https://doi.org/10.1179/sic.2006.51.2.123.

Kyriakou, Y., Meyer, E., Prell, D., Kachelrieß, M., 2010. Empirical beam hardening correction (EBHC) for CT. Med. Phys. 37, 5179–5187. https://doi.org/10.1118/1.3477088.

McKinley, J.I., 1994. Bone fragment size in british cremation burials and its implications for pyre technology and ritual. J. Archaeol. Sci. 21, 339–342. https://doi.org/10.1006/jasc.1994.1033.

Minozzi, S., Giuffra, V., Bagnoli, J., Paribeni, E., Giustini, D., Caramella, D., Fornaciari, G., 2010. An investigation of Etruscan cremations by computed tomography (CT). Antiquity 84, 195–201. https://doi.org/10.1017/S0003598X00099865.

Norman, D.G., Baier, W., Watson, D.G., Burnett, B., Painter, M., Williams, M.A., 2018. Micro-CT for saw mark analysis on human bone. Forensic Sci. Int. 293, 91–100. https://doi.org/10.1016/j.forsciint.2018.10.027.

Ortner, D.J., 2003. Identification of Pathological Conditions in Human Skeletal Remains, Identification of Pathological Conditions in Human Skeletal Remains. Elsevier Inc. https://doi.org/10.1016/B978-0-12-528628-2.X5037-6.

Pankowská, A., Průchová, E., Monik, M., Nováková, M., 2014. Fines Transire Archäologische Arbeitsgemeinschaft Ostbayern / West- und Südböhmen / Oberösterreich Archeologická pracovní skupina východní Bavorsko / západní a jižní Čechy / Horní Rakousko. Fines Transire 23, 2014 19, 223–231.

Suuronen, J.P., Kallonen, A., Eik, M., Puttonen, J., Serimaa, R., Herrmann, H., 2013. Analysis of short fibres orientation in steel fibre-reinforced concrete (SFRC) by X-ray tomography. J. Mater. Sci. 48, 1358–1367. https://doi.org/10.1007/s10853-012-6882-4.

Symes, S.A., Chapman, E.A., Rainwater, C.W., Cabo, L.L., Myster, S.M.T., 2010. Knife and Saw Toolmark Analysis in Bone: A Manual Designed for the Examination of Criminal Mutilation and Dismemberment. Vasa 1–49.

Thompson, T.J.U., Gonçalves, D., Squires, K., Ulguim, P., 2017. Thermal Alteration to the Body, in: Taphonomy of Human Remains: Forensic Analysis of the Dead and the Depositional Environment. John Wiley & Sons, Ltd, pp. 318–334. https://doi.org/10.1002/9781118953358.ch21.

Traversari, M., Figus, C., Petrella, E., Piciucchi, S., Vazzana, A., Cilli, E., Saragoni, L., Benazzi, S., 2019. Paleopathological analysis of a probable case of Jarcho-Levin syndrome from the 18th century Northern Italy. Med. Hist. 3, 39–45.

Urcia, A., Zambruno, S., Vazzana, A., Anderson, M., Darnell, C.M., 2018. Prototyping an egyptian revival. Laser scanning, 3D prints and sculpture to support the Echoes of Egypt exhibition. Archeol. e Calc. 29, 317–332. https://doi.org/10.19282/ac.29.2018.24.

Van Gompel, G., Van Slambrouck, K., Defrise, M., Batenburg, K.J., De Mey, J., Sijbers, J., Nuyts, J., 2011. Iterative correction of beam hardening artifacts in CT. Med. Phys. 38, 1–31. https://doi.org/10.1118/1.3577758.

Vazzana, A., Scalise, L.M., Traversari, M., Figus, C., Apicella, S.A., Buti, L., Oxilia, G., Sorrentino, R., Pellegrini, S., Matteucci, C., Calcagnile, L., Savigni, R., Feeney, R.N.M., Gruppioni, G., Benazzi, S., 2018. A multianalytic investigation of weapon-related injuries in a Late Antiquity necropolis, Mutina. Italy. J. Archaeol. Sci. Reports 17, 550–559. https://doi.org/10.1016/j.jasrep.2017.12.009.

Villinger, C., Gregorius, H., Kranz, C., Höhn, K., Münzberg, C., Von Wichert, G., Mizaikoff, B., Wanner, G., Walther, P., 2012. FIB/SEM tomography with TEM-like resolution for 3D imaging of high-pressure frozen cells. Histochem. Cell Biol. 138, 549–556. https://doi.org/10.1007/s00418-012-1020-6.

Vincenzutto, D., Faresin, E., Salemi, G., 2016. Necropoli del Piovego (VI-IV sec. a.C.). L'utilizzo della tomografia assiale computerizzata e della fotogrammetria nel microscavo dei complessi tombali: il caso della tomba 112, in: Cividini, T., Tasca, G. (Eds.), The Funerary in Friuli and Surrounding Regions between Iron Age and Late Antiquity Atti Del Convegno InternazionaleProceedings of the International Conference(San Vito Al Tagliamento, 14 Febbraio 2013). BAR International Series 2795, Oxford, pp. 197–202.

Walker, P.L., Miller, K.W.P., Richman, R., 2008. Time, Temperature, and Oxygen Availability: An Experimental Study of the Effects of Environmental Conditions on the Color and Organic Content of Cremated Bone, in: The Analysis of Burned Human Remains. Elsevier Ltd, pp. 129–135. https://doi.org/10.1016/B978-012372510-3.50009-5.

Waterhouse, K., 2013. The effect of weather conditions on burnt bone fragmentation. J. Forensic Leg. Med. 20, 489–495. https://doi.org/10.1016/j.jflm.2013.03.016.

White, T., Folkens, P., 2005. The Human Bone Manual, The Human Bone Manual. Elsevier Inc. https://doi.org/10.1016/C2009-0-00102-0.